Bone Reports 6 (2017) 26–33

Contents lists available at ScienceDirect

Bone Reports

journal homepage: www.elsevier.com/locate/bonr

Long-term treatment with odanacatib maintains normal trabecular biomechanical properties in ovariectomized adult monkeys as demonstrated by micro-CT-based finite element analysis

Antonio Cabal *, Donald S. Williams, Richa Y. Jayakar, Jingru Zhang, Swanand Sardesai, Le T. Duong

MerckSharp and Dohme Corp., Whitehouse Station, NJ, USA

ARTICLE INFO

Article history:
Received 5 October 2016
Received in revised form 5 January 2017
Accepted 6 January 2017
Available online 7 January 2017

Keywords:
Odanacatib
Finite element analysis
micro-CT

ABSTRACT

The cathepsin K inhibitor odanacatib (ODN) is a potent and reversible inhibitor of osteoclastic resorption activity. This drug is currently under development for the treatment of postmenopausal osteoporosis. Previously, we described data on the treatment efficacy of ODN in a preclinical estrogen-deficient model of an ovariectomized (OVX) rhesus monkey using HR-pQCT based finite element analysis (FEA) in vivo estimates of bone strength on the distal radius. To support the bone safety profile of ODN, we report ex vivo data on the apparent and hard tissue biomechanical properties of the trabecular bone of vertebrae of animals after 20 months of dosing in three treatment groups: Vehicle (VEH), ODN (2 mg/kg/day), and ALN (30 μg/kg/week).

Biomechanical axial compression tests were performed on cylindrical trabecular samples cored out of the third lumbar vertebra of each animal at the end of the study. The biomechanical test results demonstrated that a normal (positive correlation between bone mineral density and bone strength) apparent material property relationship was maintained in the lumbar spine of ODN and ALN treated non-human primates (NHP). Trabecular bone hard tissue Young's modulus value was estimated using experimentally measured stiffness combined with FEA. The FEA and experimental results demonstrated that ODN treatment for 20 months maintained normal trabecular bone material hard tissue properties in the OVX-monkeys and was comparable to ALN.

1. Introduction

Osteoporosis results from an imbalance between bone resorption and bone formation, when bone resorption outweighs formation. The resulting low bone mineral density (BMD) and accompanying microarchitectural deterioration lead to increased skeletal fragility and an increased risk of fracture (NIH Consensus Development Panel on Osteoporosis Prevention, Diagnosis, and Therapy, 2001). The most commonly used drugs for the treatment of osteoporosis are the inhibitors of bone resorption (antiresorptives), including bisphosphonates, selective estrogen receptor modulators and the RANK ligand neutralizing antibody denosumab (Baron et al., 2011).

Cathepsin K (CatK), the most abundant cysteine protease expressed in osteoclasts, is primarily responsible for the degradation of bone matrix necessary for bone resorption. Deficiency of CatK activity in humans causes a rare autosomal recessive bone sclerosing disorder called pycnodysostosis (Gelb et al., 1996). Affected individuals are typically short in stature and, in spite of dense bones, suffer from increased non-traumatic fractures. Disruption of the CatK gene in mice produced a phenotype of high bone mass (Duong, 2012); however, the effect on gene deletion of CatK on bone biomechanical properties in mice seems to be strain dependent (Pennypacker et al., 2009). Even if the poor bone quality in affected individuals could be due to the life-long defect of CatK during growth, it is important to address the impact of long-term pharmacological effects of a CatK inhibitor on bone material properties in adult patients.

Several CatK inhibitor drug candidates, relacatib, balicatib, odanacatib (ODN) and ONO-5443 have been evaluated for safety and efficacy in humans (Bromme and Lecaille, 2009); however, ODN is the only clinical candidate that advanced into Phase III development for the treatment of postmenopausal osteoporosis. ODN is an orally active, potent, and selective CatK inhibitor which potently inhibits human CatK enzyme activity (IC_{50} = 0.20 nM) and has ≥300-fold selectivity against all other known human cathepsins (Gauthier et al., 2008). The five-year Phase II trial demonstrated progressive dose-dependent increases in BMD in postmenopausal women with low BMD (Bone et al., 2010;

* Corresponding author at: Quantitative Pharmacology & Pharmacometrics, Merck Research Laboratories, North Wales, PA 19454, USA.
E-mail addresses: antonio.cabal@merck.com (A. Cabal), donald.williams686@gmail.com (D.S. Williams), richa_jayakar@merck.com (R.Y. Jayakar), ruharvard@gmail.com (J. Zhang), swanuteju@yahoo.com (S. Sardesai), leduong57@gmail.com (L.T. Duong).

http://dx.doi.org/10.1016/j.bonr.2017.01.001

Eisman et al., 2011; LangdahlB et al., 2012). In the randomized, placebo-controlled, double-blinded, even-driven, Phase 3 Long-Term Odanacatib Fracture Trial (LOFT; NCT00529373) (Bone et al., 2015), the planned analysis after 5-years of therapy has demonstrated that ODN 50-mg once-weekly continuously increases bone mass and significantly reduced the risk of osteoporotic spine, hip and non-vertebral fractures in post-menopausal women with osteoporosis as compared to those on placebo (McClung et al., 2014; Duong et al., 2016).

As a novel therapeutic for the treatment of osteoporosis, it is necessary to investigate the long-term treatment effects of ODN on the quality of bone. The importance of assessing the bone safety profile of osteoporosis drugs is exemplified by sodium fluoride treatment where increased bone mass was accompanied by increased fragility of bone (Riggs et al., 1990a; Sogaard et al., 1994a; Jiang et al., 1996a). At the tissue level, structural integrity of whole bones has contributions from the total bone mass, the macro and micro architecture of bone, and the properties of the constituent tissue (Meulen et al., 2001). However, the only available clinical assessment for diagnosis of osteoporosis as well as evaluation of fracture risk in osteoporotic patients is currently limited to the measurement of bone mineral density (BMD). Therefore, pre-clinical studies to assess the long-term treatment effects of a bone drug on the quality of bone have remained a requirement for drug approval (FDA, 1994 Guidelines). Moreover, animal studies allow testing in the same skeletal site for multiple bone quality metrics, including bone mass by DXA, macro- and micro- architecture by low and high resolution computer tomographic imaging methods, and ex vivo measurements of biomechanical strength, composition of bone tissue, and detailed histomorphometry (Balena et al., 1993b).

The efficacy and bone safety of CatK inhibitors have been studied in estrogen-deficient non-human primates and rabbits (Pennypacker et al., 2011; Jerome et al., 2011; Ochi et al., 2011). In these studies, CatK inhibitors significantly reduced bone resorption while relatively preserving bone formation, resulting in both increased BMD and bone strength (Duong, 2012). Previously, ODN dosed in prevention mode at subclinical exposures has been demonstrated to effectively prevent bone loss and increased bone strength in the estrogen-deficient model of ovariectomized (OVX) rhesus monkeys treated for 21 months (Pennypacker et al., 2014). In that study, ODN treatment decreased trabecular remodeling of the spine and hip, but promoted endocortical modeling-based bone formation in the hip of OVX-monkeys (Pennypacker et al., 2014). In addition, ODN stimulated periosteal bone formation in the femoral neck, proximal and central femur (Pennypacker et al., 2014).

More recently, a second study in OVX-rhesus monkeys also dosed with ODN in prevention mode for 20-months provided drug plasma exposures that approximated or exceeded the clinical exposure of the 50-mg once-weekly dose in humans (Williams et al., 2013). It demonstrated that treatment protected BMD of spine and hip to levels comparable with alendronate (ALN)-treated OVX-monkeys, while improving cortical thickness of long bones significantly above to that with ALN (Williams et al., 2013). The same study also described in vivo data on the treatment efficacy of ODN in OVX-rhesus monkeys using HR-pQCT based finite element analysis (FEA) in vivo estimates of bone strength on the distal radius (Cabal et al., 2013). To further support the bone safety profile of ODN, we report here ex vivo analysis on the apparent (experimentally determined on whole trabecular core) and hard tissue (intrinsic of bone material) biomechanical properties of the trabecular bone of vertebrae of animals in the above mentioned study after 20 months of dosing. A control vehicle treated group and an active comparator alendronate treated group are also included. The high resolution images obtainable from ex vivo micro-CT allow the generation of more accurate meshes for FEA estimation of mechanical properties of the vertebral trabecular bone to evaluate ODN treatment effect on bone hard tissue Young's modulus.

2. Methods

2.1. Animals and study design

All procedures were approved by the Institutional Animal Care and Use Committee of Merck Research Laboratories. The in-life study design, baseline characteristics, in-life areal and volumetric bone mineral density (BMD), and bone turnover markers have been previously described (Williams et al., 2013). Briefly, 64 female rhesus monkeys (*Macaca mulatta* 12–22 years of age) were randomized into 4 groups according to femoral neck aBMD and 1/3 distal radial Ct.Th. Ten days after bilateral OVX, the 4 groups were dosed with: (1) Vehicle (VEH) containing novel formulation hydroxypropyl methyl cellulose acetate succinate (HPMC-AS) polymer; (2) ODN at 2 mg/kg, (L-ODN, p.o., q.d.); (3) ODN at 8 mg/kg (H-ODN, p.o., q.d.); (4) ALN at 30 μg/kg/week (15 μg/kg twice weekly, s.c.). The ALN subcutaneous dose was selected to produce an approximate plasma concentration in the monkeys equaling that of ALN 70-mg oral and once-weekly clinical dose, taking into account the oral bioavailability of 0.75% in humans (Balena et al., 1993a). ODN was dosed in the same HPMC-AS formulation. L-ODN dose provided the mean daily exposure of ODN (AUC_{0-24}) in plasma was ~12 $\mu M \cdot h_{0-24}$ which was ~1.8-fold of the daily clinical exposure as estimated from the ODN 50-mg once-weekly. H-ODN dose at 8 mg/kg/d provided mean daily exposure of ODN at 142 $\mu M \cdot hr_{0-24}$. This dose group was therefore adjusted to ODN 4 mg/kg/day after 5.5 months of dosing to target a steady state exposure of 51 $\mu M \cdot hr_{0-24}$ or 7.8 times the clinical exposure for the rest of the study duration. Because the H-ODN group was included for a toxicology study, this group was not subjected to the exploratory high resolution imaging of the study reported here. Animals were euthanized at 20 months, lumbar vertebrae (LV3–5) were harvested for ex-vivo imaging and biomechanical testing.

2.2. Specimen preparation and imaging

The third lumbar vertebrae (LV3) were excised for ex-vivo μCT imaging. The LV3 were scanned at an isotropic 20 μm resolution using a Scanco μCT-35 scanner (Scanco Medical AG, Brütisellen, Switzerland). The first step in the bone coring process was to estimate the average surface area available for cylindrical coring from the center slice of the μCT scans in order to avoid the vertebral vein space during coring. The location of the core was determined by positioning a 4.25 mm diameter circle on the full vertebral body μCT image center slice as described in Fig. 1A.

A computer numerical control (CNC) Sherline milling machine was fitted with a water bath to enable coring of the vertebral body bone under water (Fig. 1B). The frozen bone sample was first thawed in saline solution to bring to room temperature. The vertebral body was prepared for coring by cutting off the processes. The bone length (in the z-direction) was then measured using calipers. Specimens were cored such that the main trabecular orientation was aligned with the axis of the cylinder. The Sherline milling machine was programmed to perform a peck drilling code. The code was programmed such that the bone was cored 0.04 mm above its base in ten small steps. This was done to avoid coring all the way through the disc material causing the core to become lodged in the coring bit.

Once the coring was completed, the entire vertebral body was removed from the water tub and the core was pushed out gently from bone using a narrow steel rod. All the cores were then scanned at an isotropic 12 μm resolution using a Scanco μCT-35 scanner. Fig. 1C shows a typical μCT image of a lumbar vertebral core. Before endcapping the cores for compression testing, they were cleaned using a water jet to remove marrow and blood. The bone cores were then dried using compressed air, and fitted and glued into brass endcaps using Loctite 401 (Keaveny et al., 1994). The bones were then wrapped in plastic film to preserve the bone moisture and stored in a refrigerator until performing

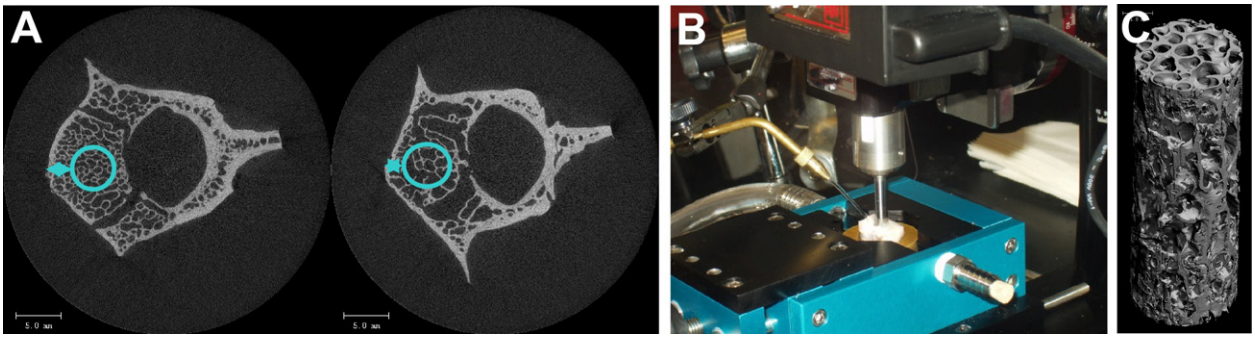

Fig. 1. Preparation of trabecular core specimen. (A). Representative μCT images of third lumbar vertebrae (LV3) at 20 μm isotropic resolution from two animals. The images are used to estimate the average surface area available for cylindrical coring in order to avoid the vertebral vein space. (B). A trabecular bone cylinder was cored under water using a computer controlled Sherline milling machine. (C). A mCT image of a core at 12 μm isotropic resolution.

compression testing. The bone cores were tested as wet bone, not in a dehydrated state.

2.3. Biomechanical testing

The endcapped cores were compressed using the MTS Alliance RT/50 machine (see Fig. 2A) to record the loads and displacement. The endcapped cores were place between the two fixtures on the MTS Alliance RT/50 actuator using key type chucks as shown in Fig. 2A. Three preconditioning cycles to 0.1% strain were followed by a final ramp at 0.5% strain per second that loaded the specimen all the way to failure (Morgan and Keaveny, 2001). The force and deformation data was recorded for each experiment and the experimental stiffness was computed as the initial linear slope of the force-deformation curve (Fig. 2B). The experimental stress was computed for each specimens using the average of cross-sectional areas of each slice that formed the specific animal μCT image. A representative stress-strain curve is shown in Fig. 2C (effective length as defined in (Keavery et al., 1997)). The Apparent Young's Modulus was computed as the initial linear slope of the stress-strain curve (Fig. 2C).

2.4. Finite element analysis (FEA)

Finite element (*FE*) models were generated from the μCT images of the cores and subsequently used in the estimation of the trabecular bone hard tissue Young's Modulus in-silico, as illustrated in Fig. 4. The images had a 12 μm isotropic voxel size, making the files too large for reasonable CPU demands, and it was necessary to coarsen the mesh to run the *FE*-simulations in ANSYS Mechanical (ANSYS Inc.) in a realistic time frame of a few hours (as opposed to a number of days with the original resolution) using 6 nodes of a 13-node dual-core 64-bit Linux

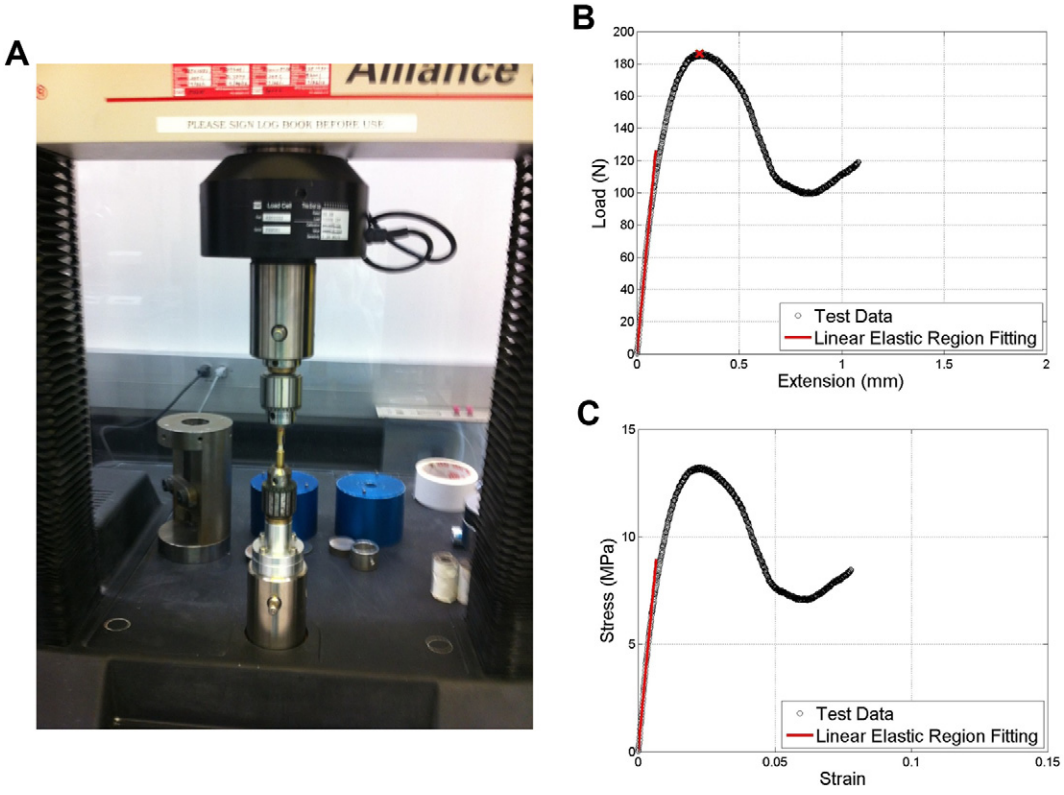

Fig. 2. Biomechanical testing of trabecular core. (A) The cores were endcapped and compressed to failure under water at 0.5% strain per second, and load-displacement curves were recorded. Typical curves for (b) Load vs extension and (C) Stress vs Strain indicating the linear elastic region (red line) and the Peak force (red x) used for biomechanical property calculations.

cluster with 2.66 GHz processors, 48 GB of RAM on the master node, and 16 GB RAM per 2-processor node.

Downsampling the images via merging the individual pixels can bring about averaging of the merged pixels and produce changes in the bone volume (*BV*) of the downsampled image. The bone morphology and *BV* are important determinants of bone strength, and thus it is imperative to maintain a constant value of *BV* in the downsampling process. This was accomplished using an adaptive threshold that preserved the *BV* of the parent images. Two different test thresholds were first applied: a lower one that gave a *FE*-volume with a *BV* above that for parent images and a higher one that gave a *FE*-volume below the original *BV*. The threshold corresponding to the *FE*-volume with *BV* of parent image was then determined from a linear interpolation of the two test thresholds. The resulting *FE*-volume corresponding to 20 μm voxel size matched within 1% the BV of the original parent image.

FE-models were created on the downsampled images using ANSYS Mechanical (ANSYS, Inc.) assuming a homogeneous linear–elastic isotropic material (Young's modulus $E = 12$ GPa; Poisson's ratio $\nu = 0.3$). A fixed displacement was applied on the top side wall nodes of the core, the location where the core was affixed in the top brass endcap. The nodes corresponding to the location where the core was affixed in the bottom brass endcap were clamped.

2.5. Statistics

Data are shown as means ± the standard deviation (SD). The homogeneity of the group variances was evaluated using the Levene test at the 0.05 significance level. If differences between group variances were not found to be significant ($p > 0.05$), then a one way analysis of variance (ANOVA) was performed followed by Dunnett's multiple comparison test to compare each treatment with the VEH group. Differences were considered significant in the control Dunnett's test when $p < 0.05$.

If Levene's test indicated heterogeneous group variances ($p \leq 0.05$), then the non-parametric comparison with control was performed using the Steel Method (Steel, 1959). Each group was compared to the control group (α of 5% was considered significant).

3. Results

3.1. Effect of ODN on vertebral bone density and microarchitecture

Table 1 summarizes the bone density and microarchitecture parameters obtained from microCT images of the trabecular LV3 cores, together with the biomechanical properties. The 3D microarchitectural parameters Tb.N, Tb.Th. and Tb.Sp showed only slight changes with no statistically significant signal. We used Dunnetts multiple comparisons test for means comparisons to the VEH group. High resolution CT imaging results of the trabecular cores show a trend of higher but not statistically significant vBMD in the ALN ($p = 0.07$) and ODN ($p = 0.3$) groups. Animals in this study were also subjected to regular in vivo imaging of the spine using DXA and QCT, and data have been reported in a previous publication (21). At 18 months, vBMD of trabecular bone in vertebrae averaged over LV3–LV5 obtained from QCT demonstrated a higher vBMD compared to VEH for ODN ($p < 0.01$) and ALN ($p < 0.01$). At 18 months, aBMD of the whole vertebrae at averaged over LV1-LV4 using DXA demonstrated a higher aBMD compared to VEH for ODN ($p < 0.001$) and ALN ($p < 0.001$).

Table 1
Density and geometry parameters for OVX + VEH, OVX + ALN and OVX + ODN groups; mean ± SD.

Group	OVX vehicle	ODN 2 mg/kg	ALN 30 μg/kg/wk
Specimens (N)	14	15	15
Peak force (N)	120.68 ± 18.02	122.57 ± 28.19	138.66 ± 38.34
Stiffness (N/mm)	1026.96 ± 207.78	1069.02 ± 185.33	1160.58 ± 233.44
Trab. vBMD (mg HA/cm^3)	392.13 ± 40.20	425.53 ± 50.81	443.29 ± 91.91
Trab. BMC (mg HA/mm)	5.63 ± 0.58	6.11 ± 0.73	6.30 ± 1.24
Trab. BV/TV	0.236 ± 0.038	0.260 ± 0.047	0.276 ± 0.090
Trab. number (1/mm)	2.055 ± 0.179	2.186 ± 0.286	2.182 ± 0.250
Trab. thickness (mm)	0.119 ± 0.018	0.119 ± 0.023	0. 127 ± 0.033
Trab. separation (mm)	0.457 ± 0.040	0.436 ± 0.059	0.428 ± 0.043
Peak stress (MPa)	8.11 ± 1.29	8.54 ± 1.98	9.70 ± 2.74
Apparent modulus (MPa)	886.30 ± 166.97	969.49 ± 162.76	1078.49 ± 224.93*
Tissue modulus (GPa)	5.61 ± 0.72	5.91 ± 0.76	5.52 ± 0.96

* $p < 0.05$ with OVX-Veh as control group for Dunnettt's test.

3.2. Effect of ODN on bone quality

There was a strong positive correlation ($r = 0.77$, F-Ratio $p < 0.0001$) between volumetric bone mineral density (*vBMD*) and *peak force* (maximum of the load-deformation curve shown in Fig. 3A reached during biomechanical trabecular core bone compression testing Fig. 2B). Fig. 3B shows a similarly strong linear relationship ($r = 0.73$, F-Ratio $p < 0.0001$) between bone volume fraction (*BV/TV*) and peak force. Regressions had similar slopes across all groups, with ODN and VEH being closer to each other and slightly steeper than the ALN group.

Apparent Young's modulus for trabecular LV3 cores was also positively correlated with *vBMD* and *BV/TV* in all treatment groups, with slightly steeper slopes in the ODN and VEH groups. The data plotted in Fig. 3D showed that increases in *BV/TV* strongly correlate with increases in apparent Young's modulus ($r = 0.75$, F-Ratio $p < 0.0001$). The correlation between apparent Young's modulus and *vBMD* is slightly (but not significantly) stronger ($r = 0.79$, F-Ratio $p < 0.0001$) than the one exhibited between peak force and *vBMD* (Fig. 3C). An indicator variable regression with an interaction was used to compare the slopes and intercepts of the treatment group regression lines plotted in Fig. 3 for the different arms of the study. No statistically significant differences were found between the slopes of the treatment groups in any of the 4 plots shown in Fig. 3. We have evidence the regression intercepts of Peak Force ($p = 0.046$) and Apparent Modulus ($p = 0.007$) on BV/TV differ between the treatment groups; e.g. we rejected the null hypothesis that the intercepts are the same in each treatment group.

3.3. FEA and bone hard tissue properties

Using an initial bone hard tissue Young's modulus value of 12 GPa for FE modeling, the apparent stiffness was computed for each specimen. The true hard tissue Young's Modulus was estimated from the ratio of the experimental (K_{exp}) and FE-model (K_{FEM}) computed stiffness as illustrated in Fig. 4. The mean hard tissue Young's Modulus and their corresponding standard errors for each group are shown in Fig. 5. The results clearly showed only small differences between the mean Young's Modulus value of different treatment groups (ANOVA $p = 0.4$).

4. Discussion

The primary objective of this work was to evaluate the effect of long-term ODN treatment in OVX-NHP on the biomechanical properties of the trabecular bone of vertebrae. Destructive biomechanical testing at different skeletal sites in a previous study have shown that long term ODN treatment even at subclinical exposures improved structural strength of the femoral midshaft (Pennypacker et al., 2014) and femoral neck (Cusick et al., 2012), improved bone strength in the ultradistal radius (Cabal et al., 2013), and maintained normal bone strength at the spine in estrogen-deficient monkeys (Masarachia et al., 2012). The increased strength in these skeletal sites, particular in the lumbar vertebra, was accompanied by an increase in BMD, suggesting that increases in bone mass by ODN treatment may have led to an increase in bone strength, thus preserving bone quality in all of these skeletal

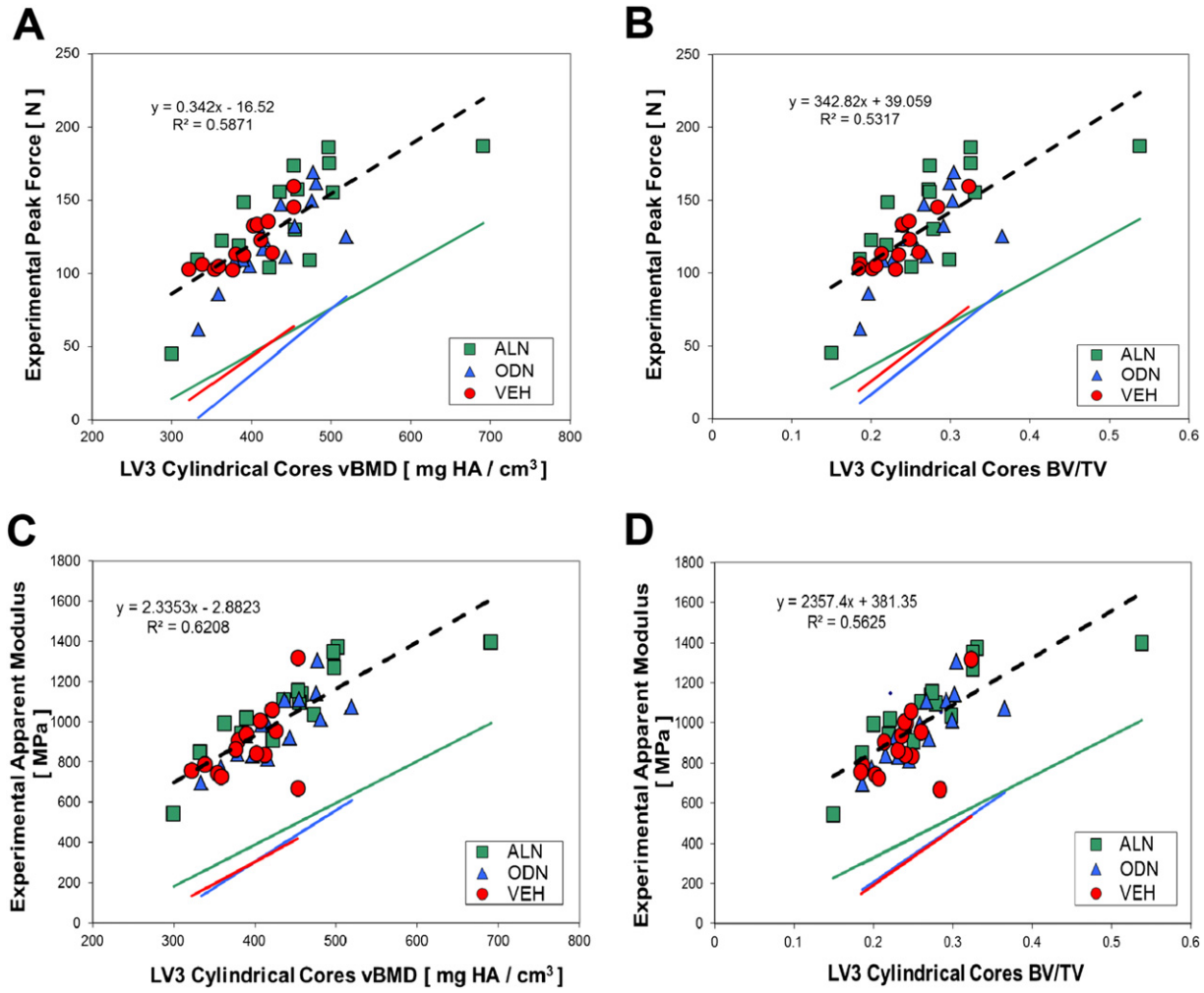

Fig. 3. Relationship of biomechanical properties of the cylindrical trabecular core to common measurements of bone mass determined from μCT images. Effect of (A) volumetric BMD (vBMD, mg HA/cm^3), and (B) bone mineral content (BMC, mg HA/mm), on the Peak Force to Failure (N). (C) Effect of BV/TV on the experimentally determined Young's Modulus.

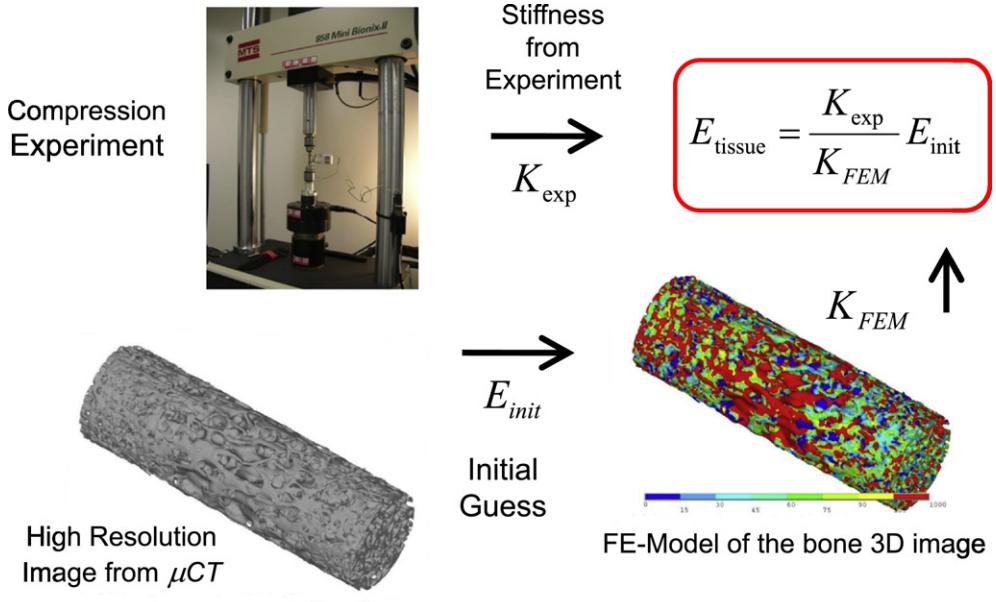

Fig. 4. Schematic of the methodology used to estimate the hard tissue Young's Modulus from the experimentally determined stiffness and the FEA-computed stiffness.

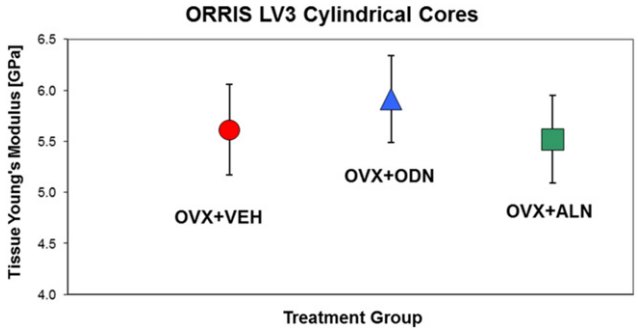

Fig. 5. Estimated hard tissue Young's Modulus (GPa) of trabecular tissue in the OVX + VEH, OVX + ALN and OVX + ODN groups. Error bars represent the standard error of the mean (SEM).

sites (Pennypacker et al., 2014; Cabal et al., 2013; Cusick et al., 2012; Masarachia et al., 2012; Williams et al., 2013).

Long-term treatment with sodium floride has been known to result to poor bone quality associated with its use for the treatment of osteoporosis. Riggs and coworkers (Riggs et al., 1990b) found after a four-year treatment with sodium floride, the postmenopausal women in their study had on average a 35% increase in lumbar spine BMD but there was no fracture risk reduction in the spine of treated women compared to the placebo group. A later publication (Sogaard et al., 1994b) provided support for these findings using iliac crest biopsies on the same patients before and after a 5-year osteoporosis treatment with sodium fluoride. The authors found a trabecular bone strength reduction of about 50% compared with pretreatment biopsies. Preclinical work in rats (Jiang et al., 1996b) confirmed the conclusions regarding the discrepancy between increases in bone mass and the expected increase in bone strength. Results from the work presented here directly assess the treatment-related impact on bone quality in preclinical models prior to clinical outcomes in support of the regulatory requirement guidance for the development of new osteoporosis drugs (FDA, 1994 Guidelines; Colmna, 2003).

The biomechanical properties mentioned above are extrinsic properties as they were determined on the whole, or sections of the intact skeletal site, and therefore were dependent on several factors of the tested specimen such as overall shape, size, cortical:trabecular bone mass. The hard bone tissue Young's Modulus examines if ODN treatment causes any undesired changes to the bone tissue's material characteristics; ideally, osteoporosis treatment reduces fracture risk by increasing bone mass and not by altering the intrinsic mechanical properties of bone. Direct measurement of intrinsic bone biomechanical properties can give insight into changes to its structural integrity at the level of the biomechanical properties of the tissue per se, but this ideally requires testing of the particular bone type in isolation from its host structure. Intrinsic tissue material properties of cortical bone have been made using techniques such as three-point bending or nano-indentation, but application of these methods to trabecular bone is considerably more difficult due primarily to the experimental challenges imposed by the small dimensions of individual trabeculae (Guo, 2001). However, preparing a cylindrical core of the trabecular scaffold and measuring its biomechanical properties are relatively easier to achieve, but still provides biomechanical properties relating to trabecular tissue, albeit an 'apparent' value because it is measured in the host trabecular network. We performed biomechanical axial compression of cylindrical trabecular samples cored out of the third lumbar vertebra of each animal at the end of the study. The elastic properties of the trabecular bone hard tissue were obtained using an scaling procedure using the biomechanical compression data of the trabecular cores and FEA using micro-CT images of the cores. We used this approach to experimentally measure the 'apparent' trabecular tissue properties, and back-calculate the trabecular bone intrinsic tissue material properties using *FEA* (Hou et al., 1998; Ladd et al., 1998; Bevill et al., 2009).

We adopted here the operational definition of bone quality proposed and used by other authors (Hernandez and Keaveny, 2006; Ominsky et al., 2011). Bone quality is considered to group the features of a bone, independent of mass, that influence its strength. The existing whole bone morphology evidence about the bone quality in the spine of ODN treated OVX-NHP was expanded using trabecular cores specimens tested in compression. These data allow us to isolate pure trabecular bone and evaluate its biomechanical performance independently of the whole bone, including the vertebral cortex. In doing so we investigated whether ODN treatment had any bone quality impact in bone volume fraction and hard tissue properties at the microarchitectural level. An important background information to keep in mind here are the findings from Homminga et al. (2002) who showed no significant differences in the proximal femora trabecular bone hard tissue Young's modulus between patients with and without hip fractures.

The positive linear correlation exhibited by all the arms of the study in the strength-density relationship displayed in Fig. 3A led us to conclude that, unlike sodium fluoride, neither ALN or ODN altered bone quality in NHP in any way that would depict negative clinical implications. Thus, increases in *vBMD* correspond with linearly proportional increases in bone strength which support the normal bone quality hypothesis, i.e. bone biomechanical performance can be assessed and quantified from bone density. Fig. 3B shows that bone strength has increases that are commensurate with increases in bone volume fraction (*BV/TV*), which, given the direct proportionality between *BV/TV* and bone apparent density, supports the findings of long-term ODN treatment preserving normal bone quality in the spine microarchitecture.

The positive correlations found between apparent Young's modulus along the main loading orientation of the tested specimens plotted as a function of *vBMD* in Fig. 3C and as a function of *BV/TV* in Fig. 3D provide intrinsic data support for the preservation of bone quality in all arms of the study. A step further in the evaluation of intrinsic properties was performed using *μFEA* following the procedure illustrated in the schematic of Fig. 4. The key assumption here is that the ratio between the apparent stiffness measured during the compression tests and the *μFEA*-estimated stiffness is equal to the ratio of the respective tissue Young's moduli, as shown in the schematic of Fig. 4 (Hou et al., 1998; Ladd et al., 1998; Bevill et al., 2009; Homminga et al., 2002). We found only minor differences between the mean hard tissue elastic-modulus value of different treatment arms which are not statistically significant ($p = 0.4$) as shown in Fig. 5. Only one parameters for the ALN group (see Table 1) reached statistically significant differentiation ($p < 0.05$) from the VEH group: apparent elastic-modulus.

This study assessed the long-term effects of the CatK inhibitor ODN on hard tissue biomechanical properties of OVX NHP vertebral trabecular bone after 20 months of dosing. The results indicate that long-term treatment with ODN maintains normal trabecular bone material hard tissue properties in the OVX-monkeys and was comparable to ALN. These findings are consistent with the existing preclinical data showing ODN maintained normal bone strength at the spine of treated OVX-NHP and clinical evidence showing ODN significantly reduced fracture risk in postmenopausal women with osteoporosis and led to progressive increases in BMD at the lumbar spine and hip compared with placebo for ODN patients.

Despite the robust efficacy of this drug for the treatment of osteoporosis as demonstrated in the LOFT study, clinical development of the CatK inhibitor ODN was recently terminated due to an increased risk of stroke in the postmenopausal patients with osteoporosis on active ODN treatment versus a placebo group (Langdahl et al., 2012; Langdahl et al., 2015; McClung et al., 2016). To date, there is no preclinical evidence to link the inhibition of CatK to any cardiovascular risks, and it is thus unclear whether the adjudicated stroke adverse event is directly related to the CatK mechanism. Furthermore, unlike the standard antiresorptives, the bisphosphonates or denosumab, ODN blocks osteoclastic bone resorption while maintaining subsequent bone formation during bone remodeling (Duong et al., 2016). Taking into account

the overall risk-to-benefit of ODN in the aged osteoporotic population, the class of CatK inhibitors still represents a novel and potentially important therapy for the treatment of diseases, such as metastatic- or inflammatory-induced acute bone loss.

Funding source

All studies were funded completely by Merck Sharp and Dohme Corp., a subsidiary of Merck & Co., Inc.

Conflict of interest statement

Antonio Cabal and Richa Y. Jayakar are current employees; Swanand Sardesai, Jingru Zhang, Donald S. Williams and Le T. Duong were former employees of Merck & Co., Inc., who may own stock or stock options in the company

Acknowledgments

The authors would like to thank Michael Jekir and Tony Keaveny for their support and guidance in the cylindrical specimen preparation and biomechanical testing, Adan Procopio for lending his lab equipment and support for the biomechanical testing, Seth Clark for providing statistical support, Jennifer Pawlowski for her assistance and careful review of the manuscript.

References

Balena, R., Toolan, B.C., Shea, M., Markatos, A., Myers, E.R., Lee, S.C., et al., 1993a. The effects of 2-year treatment with the aminobisphosphonate alendronate on bone metabolism, bone histomorphometry, and bone strength in ovariectomized nonhuman primates. J. Clin. Invest. 92 (43), 2577–2586.

Balena, R., Toolan, B.C., Shea, M., Markatos, A., Myers, E.R., Lee, S.C., et al., 1993b. The effects of 2-year treatment with the aminobisphosphonate alendronate on bone metabolism, bone histomorphometry, and bone strength in ovariectomized nonhuman primates. J. Clin. Invest. 92, 2577–2586.

Baron, R., Ferrari, S., Russell, R.G., 2011. Denosumab and bisphophonates: different mechanisms of action and effects. Bone 48, 677–692.

Bevill, G., Eswaran, S.K., Farahmand, F., Keaveny, T.M., 2009. The influence of boundary conditions and loading mode on high-resolution finite element-computed trabecular tissue properties. Bone 44, 573–578.

Bone, H.G., McClung, M.R., Roux, C., Recker, R.R., Eisman, J.A., Verbruggen, N., Hustad, C.M., DaSilva, C., Santora, A.C., Ince, B.A., 2010. Odanacatib, a cathepsin-K inhibitor for osteoporosis: a two-year study in postmenopausal women with low bone density. J. Bone Miner. Res. 25, 937–947.

Bone, H.G., Dempster, D.W., Eisman, J.A., Greenspan, S.L., McClung, M.R., Nakamura, T., Papapoulos, S., Shih, W.J., Rybak-Feiglin, A., Santora, A.C., Verbruggen, N., Leung, A.T., Lombardi, A., 2015. Odanacatib for the treatment of postmenopausal osteoporosis: development history and design and participant characteristics of LOFT, the Long-Term Odanacatib Fracture Trial. Osteoporos. Int. 26 (2), 699–712 (Feb).

Bromme, D., Lecaille, F., 2009. Cathepsin K inhibitors for osteoporosis and potential off-target effects. Expert Opin. Investig. Drugs 18, 585–600.

Cabal, A., Jayakar, R.Y., Sardesai, S., Phillips, E.A., Szumiloski, J., Posavec, D.J., Mathers, P.D., Savitz, A.T., Scott, B.B., Winkelmann, C.T., Motzel, S., Cook, L., Hargreaves, R., Evelhoch, J.L., Dardzinski, B.J., Hangartner, T.N., McCracken, P.J., Duong, L.T., Williams, D.S., 2013 Oct. High-resolution peripheral quantitative computed tomography and finite element analysis of bone strength at the distal radius in ovariectomized adult rhesus monkey demonstrate efficacy of odanacatib and differentiation from alendronate. Bone 56 (2), 497–505.

Colmna, E.G., 2003. The Food and Drug Administration's osteoporosis guidance document: past, present, and future. J. Bone Miner. Res. 18, 1125–1128.

Cusick, T., Chen, C.M., Pennypacker, B.L., Pickarski, M., Kimmel, D.B., Scott, B.B., Duong, L.T., 2012. Odanacatib treatment increases hip bone mass and cortical thickness by preserving endocortical bone formation and stimulating periosteal bone formation in the ovariectomized adult rhesus monkey. J. Bone Miner. Res. 27 (1; 21), 524–537.

Duong, L., 2012. Therapeutic inhibition of cathepsin K reducing bone resorption while maintaining bone formation. BoneKEy Rep. 1, 8.

Duong, L.T., Leung, A.T., Langdahl, B., 2016. Cathepsin K inhibition: a new mechanism for the treatment. Calcif. Tissue Int. 98, 381–397.

Eisman, J.A., Bone, H.G., Hosking, D.J., McClung, M.R., Reid, I.R., Rizzoli, R., Resch, H., Verbruggen, N., Hustad, C.M., DaSilva, C., Petrovic, R., Santora, A.C., Ince, B.A., Lombardi, A., 2011. Odanacatib in the treatment of postmenopausal women with low bone mineral density: three-year continued therapy and resolution of effect. J. Bone Miner. Res. 26, 242–251.

FDA, 1994. Guidelines for preclinical and clinical evaluation of agents used in the prevention or treatment of postmenopausal osteoporosis. http://www.fda.gov/OHRMS/DOCKETS/98fr/04d-0035-gdl0001.pdf.

Gauthier, JY1J.Y., Chauret, N., Cromlish, W., Desmarais, S., Duong, L.T., Falgueyret, J.P., Kimmel, D.B., Lamontagne, S., Léger, S., Le Riche, T., Li, C.S., Massé, F., DJ, M.K., Nicoll-Griffith, D.A., Oballa, R.M., Palmer, J.T., Percival, M.D., Riendeau, D., Robichaud, J., Rodan, G.A., Rodan, S.B., Seto, C., Thérien, M., Truong, V.L., Venuti, M.C., Wesolowski, G., Young, R.N., Zamboni, R., Black, W.C., 2008. The discovery of odanacatib (MK-0822), a selective inhibitor of cathepsin K. Bioorg. Med. Chem. Lett. 18 (3), 923–928.

Gelb, B.D., Shi, G.P., Chapman, H.A., Desnick, R.J., 1996. Pycnodysostosis, a lysosomal disease caused by cathepsin K deficiency. Science 273 (5279), 1236–1238 (Aug 30).

Guo, X.E., 2001. Mechanical properties of cortical bone and cancellous bone tissue. In: Cowin, S.C. (Ed.), Chapter 10, Bone Mechanics Handbook, second edition CRC Press.

Hernandez, C.J., Keaveny, T.M., 2006. A biomechanical perspective on bone quality. Bone 39, 1173–1181.

Homminga, J., McCreadie, B.R., Ciarelli, T.E., Weinans, H., Goldstein, S.A., Huiskes, R., 2002. Cancellous bone mechanical properties from normals and patients with hip fractures differ on the structure level, not on the bone hard tissue level. Bone 30, 759–764.

Hou, F.L., Lang, S.M., Hoshaw, S.J., Reimann, D.A., Fyhrie, D.P., 1998. Human vertebral body apparent and hard tissue stiffness. J. Biomech. 31, 1009–1015.

Jerome, C., Missbach, M., Gamse, R., 2011. Balicatib, a cathepsin K inhibitor, stimulates periosteal bone formation in monkeys. Osteoporos. Int. 22 (2), 3001–3011.

Jiang, Y., Zhao, J., van Audekercke, R., Dequeker, J., Geusens, P., 1996a. Effects of low-dose long-term sodium fluoride preventive treatment on rat bone mass and biomechanical properties. Calcif. Tissue Int. 58, 30.

Jiang, Y., Zhao, J., van Audekercke, R., Dequeker, J., Geusens, P., 1996b. Effects of low-dose long-term sodium fluoride preventive treatment on rat bone mass and biomechanical properties. Calcif. Tissue Int. 58, 30–39.

Keaveny, T.M., Guo, X.E., Wachtel, E.F., McMahon, T.A., Hayes, W.C., 1994. Trabecular bone exhibits fully linear elastic behavior and yields at low strains. J. Biomech. 27, 1127–1136.

Keavery, T.M., Pinilla, T.P., Crawford, R.P., Kopperdahl, D.L., Lou, A., 1997. Systematic errors in compression testing of trabecular bone. J. Orthop. Res. 15, 101–110.

Ladd, A.J., Kinney, J.H., Haupt, D.L., Goldstein, S.A., 1998. Finite-element modeling of trabecular bone: comparison with mechanical testing and determination of tissue modulus. J. Orthop. Res. 16, 622–628.

Langdahl, B., Binkley, N., Bone, H., Gilchrist, N., Resch, H., Rodriguez Portales, J., Denker, A., Lombardi, A., De Tilleghem, C.L.B., DaSilva, C., Rosenberg, E., Leung, A., 2012. Odanacatib in the treatment of postmenopausal women with low bone mineral density: five years of continued therapy in a phase 2 study. J. Bone Miner. Res. 27, 2251–2258.

Langdahl, B., et al., 2015. Effect of odanacatib on bone density and estimated bone strength in postmenopausal women: a CT-based substudy of the phase 3 Long-Term Odanacatib Fracture Trial (LOFT). J. Bone Miner. Res. 30 (Suppl. 1).

LangdahlB, B.N., BoneH, G.N., Resch, H., Rodriguez, P.J., Denker, A., Lombardi, A., Le Bailly, D.T., DaSilva, C., Rosenberg, E., Leung, A., 2012. Odanacatib in the treatment of postmenopausal women with low bone mineral density: five years of continued therapy in a phase 2 study. J. Bone Miner. Res. 27 (1), 2251–2258.

Masarachia, P.J., Pennypacker, B.L., Pickarski, M., Scott, K.R., Wesolowski, G.A., Smith, S.Y., Samadfam, R., Goetzmann, J.E., Scott, B.B., Kimmel, D.B., Duong, L.T., 2012. Odanacatib reduces bone turnover and increases bone mass in the lumbar spine of skeletally mature ovariectomized rhesus monkeys. J. Bone Miner. Res. 27 (2; 19), 509–523.

McClung, M., et al., 2014. Odanacatib anti-fracture efficacy and safety in postmenopausal women with osteoporosis. Results from the phase III Long-Term Odanacatib Fracture Trial (LOFT). J. Bone Miner. Res. 29 (Suppl. 1).

McClung, M., et al., 2016. Odanacatib efficacy and safety in postmenopausal women with osteoporosis: 5-year data from the extension of the phase 3 Long-Term Odanacatib Fracture Trial (LOFT). J. Bone Miner. Res. 31 (Suppl. 1).

Meulen, M.C., Jepsen, K.J., Mikic, B., 2001. Understanding bone strength: size isn't everything. Bone 29, 101–104.

Morgan, E.F., Keaveny, T.M., 2001. Dependence of yield strain of human trabecular bone on anatomic site. J. Biomech. 34, 569–577.

NIH Consensus Development Panel on Osteoporosis Prevention, Diagnosis, and Therapy, 2001,. Osteoporosis prevention, diagnosis, and therapy. JAMA 285 (1), 785–795.

Ochi, Y., Yamada, H., Mori, H., Nakanishi, Y., Nishikawa, S., Kayasuga, R., Kawada, N., Kunishige, A., Hashimoto, Y., Tanaka, M., Sugitani, M., Kawabata, K., 2011. Effects of ONO-5334, a novel orally-active inhibitor of cathepsin K, on bone metabolism. Bone 49 (1), 1351–1356.

Ominsky, M.S., Stouch, B., Schroeder, J., Pyrah, I., Stolina, M., Smith, S.Y., Kostenuik, P.J., 2011. Denosumab, a fully human RANKL antibody, reduced bone turnover markers and increased trabecular and cortical bone mass, density, and strength in ovariectomized cynomolgus monkeys. Bone 49, 162–173.

Pennypacker, B., Shea, M., Liu, Q., Masarachia, P., Saftig, P., Rodan, S., Rodan, G., Kimmel, D., 2009. Bone density, strength, and formation in adult cathepsin K (−/−) mice. Bone 44, 199–207.

Pennypacker, B.L., Duong, L.T., Cusick, T.E., Masarachia, P.J., Gentile, M.A., Gauthier, J.Y., Black, W.C., Scott, B.B., Samadfam, R., Smith, S.Y., Kimmel, D.B., 2011. Cathepsin K inhibitors prevent bone loss in estrogen-deficient rabbits. J. Bone Miner. Res. 26, 252–262.

Pennypacker, B.L., Chen, C.M., Zheng, H., Shih, M.S., Belfast, M., Samadfam, R., Duong, L.T., 2014. Inhibition of cathepsin K increases modeling-based bone formation, and improves cortical dimension and strength in adult ovariectomized monkeys. J. Bone Miner. Res. 29 (8), 1847–1858.

Riggs, B.L., Hodgson, S.F., O'Fallon, W.M., Chao, E., Wahner, H.W., Muhs, J.M., et al., 1990a. Effect of fluoride treatment on the fracture rate in postmenopausal women with osteoporosis. N. Engl. J. Med. 322, 802–809.

Riggs, B.L., Hodgson, S.F., O'Fallon, W.M., Chao, E., Wahner, H.W., Muhs, J.M., et al., 1990b. Effect of fluoride treatment on the fracture rate in postmenopausal women with osteoporosis. N. Engl. J. Med. 322, 802–809.

Sogaard, C.H., Li, M., Richards, A., Mosekilde, L., 1994a. Marked decrease in trabecular bone quality after five years of sodium fluoride therapy: assessed by biomechanical testing of iliac crest bone biopsies in osteoporotic patients. Bone 15, 393–399.

Sogaard, C.H., Li, M., Richards, A., Le, M., 1994b. Marked decrease in trabecular bone quality after five years of sodium fluoride therapy: assessed by biomechanical testing of iliac crest bone biopsies in osteoporotic patients. Bone 15, 393–399.

Steel, R.G.D., 1959. A multiple comparison rank sum test: treatments versus control. Biometrics 15, 560–572.

Williams, D.S., McCracken, P.J., Purcell, M., Pickarski, M., Mathers, P.D., Savitz, A.T., Szumiloski, J., Jayakar, R.Y., Somayajula, S., Krause, S., Brown, K., Winkelmann, C.T., Scott, B.B., Cook, L., Motzel, S.L., Hargreaves, R., Evelhoch, J.L., Cabal, A., Dardzinski, B.J., Hangartner, T.N., Duong, L.T., 2013 Oct. Effect of odanacatib on bone turnover markers, bone density and geometry of the spine and hip of ovariectomized monkeys: a head-to-head comparison with alendronate. Bone 56 (2), 489–496.